Magnetic Resonance Imaging 63 (2019) 55–59

Contents lists available at ScienceDirect

Magnetic Resonance Imaging

journal homepage: www.elsevier.com/locate/mri

Original contribution

Multi-parametric MR imaging using pseudo-continuous arterial-spin labeling and diffusion-weighted MR imaging in differentiating subtypes of parotid tumors

Ahmed Abdel Khalek Abdel Razek*

Department of Diagnostic Radiology, Mansoura Faculty of Medicine, Masnoura, Egypt

ARTICLE INFO

Keywords:
Diffusion
Arterial spin labeling
Perfusion
MR imaging
Cancer
Parotid

ABSTRACT

Purpose: To evaluate multi-parametric MR imaging using pseudo-continuous arterial-spin labeling (pCASL) and diffusion-weighted imaging (DWI) in differentiating subtypes of parotid tumors.

Material and methods: This study was done on 61 consecutive patients (27 M, 34 F aged 15–75 ys: mean 42 ys) with parotid tumors that underwent pCASL and DWI with the calculation of tumor blood flow (TBF) and apparent diffusion coefficient (ADC).

Results: The mean TBF and ADC of parotid malignancy ($n = 20$) (53.1 ± 6.9 mL/100 g/min and $0.66 \pm 0.1 \times 10^{-3}$ mm^2/s) was a significant different ($P = 0.001$) than benign tumors ($n = 41$) (22.7 ± 2.7 mL/100 g/min and $1.28 \pm 0.4 \times 10^{-3}$ mm^2/s) respectively. Multi-parametric TBF and ADC were used to differentiate malignant from benign tumors has an AUC (AUC) of 0.97, and the accuracy of 90%. There was a significant difference ($P = 0.001$) TBF between Warthin tumors (WT) (26.7 ± 9.7 mL/100 g/min) and malignancy. Selection of TBF of 30.5 mL/100 g/min to differentiate malignancy from WT revealed an AUC of 0.95 and the accuracy of 87%. There was a significant difference in TBF and ADC of pleomorphic adenomas (PA) from malignancy ($P = 0.001$). Multi-parametric TBF and ADC were used to differentiate PA from parotid malignancy revealed an AUC of 1.00. There was a significant difference in TBF and ADC of PA and WT ($P = 0.001$). Multi-parametric MRI using TBF and ADC used to differentiate PA from WT have an AUC of 0.99, and the accuracy of 92%.

Conclusion: Multi-parametric MR imaging using pCASL and DWI is useful for differentiating benign parotid tumors from parotid malignancy and PA from WT and TBF helps in discrimination of WT from parotid malignancy.

1. Introduction

Characterization of parotid tumors is important for treatment planning and prognosis. Superficial parotidectomy is done for pleomorphic adenomas (PA), enucleation for Warthin tumors (WT) and total parotidectomy with radiotherapy for parotid malignancy [1–4]. The results of routine ultrasound and elastography are operator dependent [3–7]. Computed tomography and CT perfusion cannot accurately discriminate parotid tumors [2,8]. Signal intensity and pattern of contrast enhancement of parotid tumors at pre and post-contrast MR imaging cannot discriminate benign from malignant parotid tumors in most of the cases [9–10]. Diffusion-weighted imaging (DWI) is based on the Brownian motion of water protons in the tissue, which is affected by the microstructure of tissue. The apparent diffusion coefficient (ADC) helps in the differentiation of salivary tumors and misdiagnosed WT as parotid malignancy [11–14]. Recent studies added that diffusion tensor imaging cannot discriminate salivary tumors in some cases [15–16]. The main problem with DWI in the assessment of salivary tumors is discrimination of WT from malignancy. Combined dynamic contrast MR imaging and DWI may help in differentiation subtypes of salivary tumors, but there is overlap in results [17–18].

Arterial spin labeling calculates the tumor blood flow without contrast agents by application of selective inversion pulse with tagging of the inflowing spins proximal to the imaging slab. The labeled blood flows into the target tissue and the labeled blood-tissue interaction change relaxation rates of the tissue. Subtraction of labeled and unlabeled images provides a perfusion map [19–22]. The pseudo-continuous arterial spin labeling (pCASL) combines the benefits of continuous arterial spin labeling and pulsed arterial spin labeling, which utilizes a series of discrete radiofrequency pulses. pCASL have good

* Corresponding author at: Department of Diagnostic Radiology, Mansoura Faculty of Medicine, Elgomheryia Street, Mansoura 3512, Egypt.
E-mail address: arazek@mans.edu.eg.

https://doi.org/10.1016/j.mri.2019.08.005
Received 26 February 2019; Received in revised form 5 August 2019; Accepted 15 August 2019

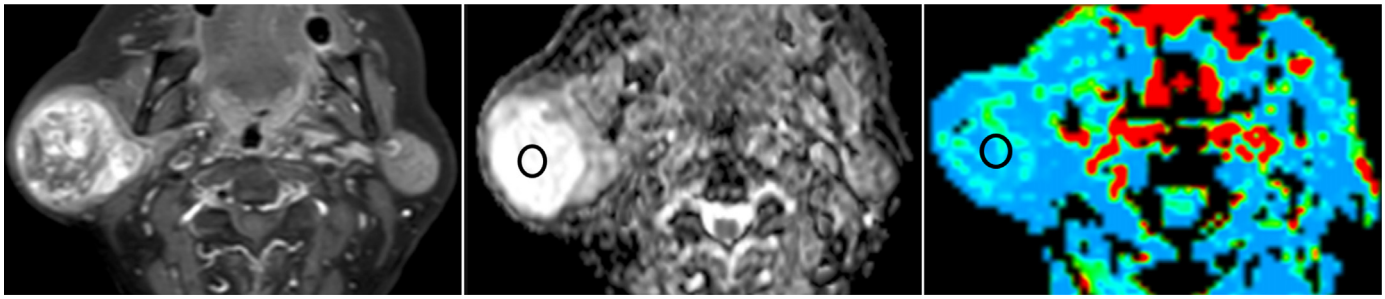

Fig. 1. Pleomorphic adenoma. (A) Axial contrast MR image shows inhomogeneous enhanced mass of right parotid gland. (B) Axial ADC map shows ROI localization with unrestricted diffusion and high ADC (1.67×10^{-3} mm^2/s). (C) ASL map shows low TBF (22.3 mL/100 g/min) of the tumor.

labeling and higher signal than continuous or pulsed arterial spin labeling [21–23]. pCASL has been used for calculation of tumor blood flow (TBF) in head and neck cancer [23–26]. TBF is a non-invasive imaging parameter that is well correlated with the pathological degree of tumor differentiation, clinical stage of the tumor and nodal metastasis of head and neck cancer [24]. There was a significant difference ($P = 0.001$) in TBF of a recurrent head and neck cancer and post-radiation changes [26]. Also, pCASL is used for evaluation of skull base [27], paranasal sinuses [28], and salivary tumors [29–31].

The rationales for the addition of pCASL to DWI in discrimination of salivary gland tumors is that DWI gives an idea about cellularity of the salivary gland tumors and pCASL gives an idea about vascularity of the tumor. Quantitative parameters of pCASL and DWI including TBF and ADC may help in the differentiation of salivary tumors without contrast medium injection.

The aim of this work was to assess multi-parametric MR imaging of parotid tumors using pCASL and DWI in differentiating subtypes of parotid tumors.

2. Material and methods

2.1. Patients

Institutional review board approval was obtained and informed consent was waived because this is a retrospective study. Retrospective analysis of 63 consecutive patients with parotid tumors was performed. Inclusion criteria were untreated patients with parotid tumors that underwent pCASL, DWI and biopsy. Two patients were excluded from the study due to susceptibility and motion artifacts at MR imaging. The final patients included in this work were 61 patients (27 male and 34 female, age ranged from 15 to 75 years; mean age 42 years). The final diagnosis was done by histological diagnoses of parotid tumors.

MR imaging.

MR imaging was done on a 1.5 Tesla scanner (Ingenia, Philips, Philips Medical Systems, Best, Netherland) with a 16-channel neurovascular coil. All patients underwent T1- (TR/TE = 800/15 ms) and T2-weighted Turbo spin-echo images (TR/TE = 6000/80 ms). The scanning parameters were: section thickness = 6 mm, inter-slice gap = 2 mm, field-of-view (FOV) = 25–20 cm and acquisition matrix = 256 × 224. Post-contrast fat-suppressed T1-weighted images were done after intravenous bolus injection of 0.1 ml/kg of body weight of gadopentetate-dimeglumine with the same scanning parameters of T1-weighted images. The contrast study was performed after DWI and pCASL.

2.2. Diffusion-weighted imaging

DWI was obtained using echo-planar imaging sequence (TR/TE = 3200/90 ms) with parallel imaging (SENSitivity Encoding [SENSE] reduction factor P 2) using a *b*-value of 0 and 1000 s/mm^2. The scanning parameters were: section thickness = 6 mm, inter-slice gap = 2 mm, FOV = 25 × 20 cm, and data matrix = 92 × 88 and scan duration = 90 s.

2.3. Pseudo-continuous arterial spin labeling

The pCASL using single-phase arterial spin labeling [26] with field echo echo-planar imaging (FEEPI) sequence was done using the labeling plane below the level of common carotid artery bifurcation. The scanning parameters were labeling duration = 1650 ms, post-label delay = 1280 ms, TR/TE = 25/20 ms, flip angle = 35 degrees, section thickness = 6 mm, inter-slice gap = 0.6 mm, NEX = one, FOV = 20 cm × 20 cm, SENSE Factor = 2.5 and scan duration = 5 min. There was a reconstruction of 2880 source images of control and labeled images. The control images were subtracted from labeled images with the formation of ASL map.

2.4. Image analysis

Image analysis was done by a radiologist (AA) with 25 years of expertise of MR imaging who was blinded to the final diagnosis. A circular region of interest (ROI) (Fig. 1) was placed on ASL map covered almost of the parotid tumor with the calculation of TBF according to the previously described equation [21] and copy of ROI was placed on ADC map with the calculation of ADC of tumors. When heterogeneous enhancement noted, the ROI was placed in the enhanced solid part of the tumor. The mean size of the ROI is 13.3 cm^2 (8.4 to 23.6 cm^2).

2.5. Statistical analysis

The statistical analysis of data was done by using the Statistical Package for Social Science version 22.0 (SPSS Inc., Chicago, Ill, USA). The mean TBF and ADC of parotid tumors were calculated. Student *t*-test was used to compare between the TBF and ADC of parotid tumors. The univariant analysis of TBF and MD of parotid tumors was done using the receiver operating characteristic curve to calculate the area under the curve (AUC). Multi-variant logistic regression analysis for multi-parametric MR imaging using TBF and ADC for differentiating malignant from benign tumors, malignant from WT, PA from WT.

3. Results

Table 1 shows mean TBF and ADC of parotid tumors. Table 2 shows the ROC curve results of TBF and ADC of parotid tumors using univariant and multivariant analysis.

The mean TBF and ADC of benign parotid tumors (Fig. 1) (22.7 ± 2.7 and 1.28 ± 0.4 × 10^{-3} mm^2/s) was significantly different ($P = 0.001$) than parotid malignancy (Fig. 2) (53.1 ± 6.9 mL/100 g/min and 0.66 ± 0.1 × 10^{-3} mm^2/s) respectively. Selection of TBF of 35 mL/100 g/min and ADC of 0.90 × 10^{-3} mm^2/s to differentiate malignant from benign parotid tumors revealed AUC of 0.93, 0.88 and accuracy of 93%, 80%, the sensitivity of 95% and 95% and

Table 1
Mean, TBF (mL/100 g/min) and ADC (10^{-3} mm^2/s) of parotid tumors.

Pathology	ADC	TBF
Malignant (*n* = 20)	**53.1 ± 6.9 (44–66)**	**0.66 ± 0.1 (0.53–0.78)**
Mucoepidermoid Carcinoma (*n* = 10)	53.1 ± 6.8 (44–66)	0.75 ± 0.1 (0.65–0.93)
Adenoid cystic carcinoma (*n* = 6)	51.1 ± 5.7 (42–58)	0.66 ± 0.1 (0.53–0.78)
Salivary duct Carcinoma (*n* = 4)	47.0 ± 2.0 (17–58)	0.70 ± 0.1 (0.58–0.79)
Benign (*n* = 41)	**22.7 ± 7.7 (16–51)**	**1.28 ± 0.4 (0.66–1.85)**
PA (*n* = 22)	19.3 ± 1.9 (16–23)	1.57 ± 0.2 (0.76–1.85)
WT (*n* = 19)	26.7 ± 9.7 (22–51)	0.83 ± 0.2 (0.66–0.95)

Table 2
ROC curve results of TBF (mL/100 g/min) and ADC (10^{-3} mm^2/s) of parotid tumors.

Parameter	Threshold value	AUC	Sensitivity	Specificity	Accuracy
Malignant Vs benign					
TBF	35.0	93	95	92	93
ADC	0.90	0.88	95	73	80
Multi-parametric		0.97	95	89	90
Malignant Vs WT					
TBF	30.5	0.95	95	78	87
Malignant Vs PA					
TBF	22.0	0.96	95	91	93
ADC	0.84	0.98	86	95	68
Multi-parametric		1.00	100	100	100
WT Vs PA					
TBF	20.5	0.91	100	58	83
ADC	1.25	0.96	94	90	92
Multi-parametric		0.99	95	95	92

specificity of 92% and 73% respectively. Multi-parametric TBF and ADC were used to differentiate benign parotid tumors from malignancy with AUC of 0.97, an accuracy of 90%, the sensitivity of 95% and specificity of 89%.

The mean TBF of WT (26.7 ± 9.7 mL/100 g/min) was significant difference ($P = 0.001$) than malignant tumors (53.1 ± 6.9 mL/100 g/min) respectively. There was insignificant difference in ADC ($P = 0.06$) between WT (0.83 ± 0.2 × 10^{-3} mm^2/s) and parotid malignancy (0.66 ± 0.1 × 10^{-3} mm^2/s). Selection of TBF of 30.5 mL/100 g/min to differentiate WT from parotid malignancy revealed AUC of 0.95, an accuracy of 87%, sensitivity of 95% and specificity of 78%.

The mean TBF and ADC of PA (19.3 ± 1.9 mL/100 g/min and 1.57 ± 0.2 × 10^{-3} mm^2/s) was significantly different ($P = 0.001$) than malignant tumors (53.1 ± 6.9 and 0.66 ± 0.1 × 10^{-3} mm^2/s) respectively. Selection of TBF of 22 mL/100 g/min and ADC of 0.84 × 10^{-3} mm^2/s to differentiate PA from malignant tumors revealed AUC of 0.96, 0.98 and accuracy of 93%, 68%, the sensitivity of 95%, 86% specificity of 91% and 95% respectively. Multi-parametric TBF and ADC were used to differentiate PA from parotid malignancy had AUC of 1.00, an accuracy of 100%, the sensitivity of 100% and specificity of 100%.

The mean TBF and ADC of PA (19.3 ± 1.9 mL/100 g/min and 1.57 ± 0.2 × 10^{-3} mm^2/s) was significantly different ($P = 0.001$) than WT (26.7 ± 9.7 mL/100 g/min and 0.93 ± 0.2 × 10^{-3} mm^2/s) respectively. Selection of TBF of 20.5 mL/100 g/min and ADC of 1.25 × 10^{-3} mm^2/s to differentiate PA from WT revealed an AUC of 0.91, 0.96, the accuracy of 83%, 92%, sensitivity of 100% and 94 and specificity of 58% and 90% respectively. Multi-parametric MRI using TBF and ADC used to differentiate WT from PA had an AUC of 0.99, an accuracy of 92%, the sensitivity of 95% and specificity of 95%.

4. Discussion

The main findings of this study are multi-parametric MRI using pCASL and DWI is useful for differentiation of benign parotid tumors from malignancy as parotid malignancy show higher TBF and lower ADC compared to benign parotid tumors. pCASL helps in differentiation parotid malignancy from WT and multi-parametric MRI using pCASL and DWI can differentiate PA from WT.

In this study, TBF of malignancy is significantly higher than that of benign tumors. This may be attributed to high vascularity, increased tumor blood volume, arterio-venous shunt formation, alter capillary transit time and increase the capillary permeability of malignancy [23,29]. One study reported that pCASL used for differentiation squamous cell carcinoma from inverted papilloma of paranasal sinuses with diagnostic accuracy of 0.92 [28]. Another study added that combined ADC and fractional anisotropy discriminate salivary malignancy from benign tumors with an accuracy of 86% [16]. One study reported that threshold percentage of dynamic susceptibility contrast (DSC%) and ADC used for differentiating malignant from benign parotid tumors is 26.5%, and 1.07 × 10^{-3} mm^2/s with an AUC of 0.96 and 0.81 respectively [19].

In this study, TBF of malignant tumors is significantly higher than that of WT with an insignificant difference in ADC. Previous studies reported there is an overlap in the ADC value between WT and malignant parotid tumors [2–3]. One study reported that the kappa coefficient for diagnosis of WT using diffusion and perfusion MR imaging for both observers is 0.79 ($P = 0.05$) [10]. One study reported that DSC% of parotid malignancy is significantly higher ($P = 0.001$) than that of WT with a threshold value of 26.9% discriminating between

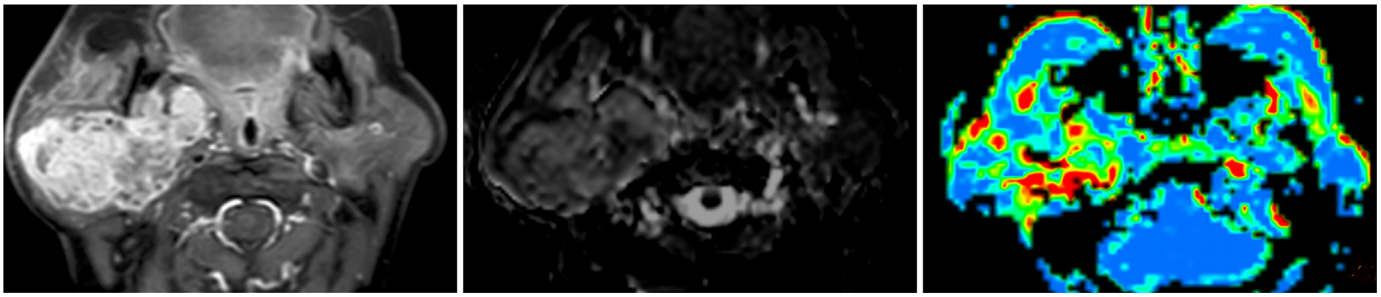

Fig. 2. Mucoepidermoid carcinoma. (A) Axial contrast MR image shows inhomogeneous enhanced mass involving the superficial and deep lobe of the right parotid gland. (B) Axial ADC map shows restricted diffusion with low ADC (0.93 × 10^{-3} mm^2/s). (C) ASL map shows high TBF (53 mL/100 g/min) of parotid malignancy.

them with an AUC of 0.99 [19]. Another study added that there is a significant difference in FA ($P = 0.001$) of WT (0.25 ± 0.07) and salivary malignancy (0.41 ± 0.07) [16].

In this study, ASL can differentiate parotid malignancy from PA. Parotid malignancy has significantly lower ADC and peak time and higher washout rate at dynamic contrast MR imaging [11]. One study reported that there is a significant difference in diffusion tensor parameter including ADC and fractional anisotropy between PA and malignant tumor ($P = 0.0012$, $P = 0.001$) [15]. Another study applied pCASL on skull base lesions found significant difference ($P = 0.001$) between median normalized-TBF for hypervascular (4.48) and non-hypervascular lesions (0.71) [27].

In this study, the TBF of PA is a significant lower than that of WT. One study reported that the median TBF of WT (95.5 mL/100 g/min) is significantly different ($P = 0.01$) than that of PA (24.5 mL/100 g/min). The cutoff TBF (60.5 mL/100 g/min) differentiate PA from WT have AUC of 0.969 and accuracy of 95.7% [29]. There is a significant difference in DSC% between PA and WT ($P = 0.001$). The threshold DSC% differentiate PA from WT is 22.5% with AUC of 0.88 [19]. Another study added signal intensity ratio on pCASL is significant higher ($P = 0.01$) in WT than PA [30].

The merits of pCASL are it does not require exogenous contrast agent, so, it used in patients with renal impairment, children and monitoring patients after therapy [20–22].

There are a few limitations to this study. First, the signals obtained from a 1.5-T scanner may not be strong enough or associated with a high signal to noise ratio for estimating TBF of parotid tumors. Further studies upon higher 3-T scanner [32,33] will improve the results. Second, this study applied pCASL and DWI for parotid tumors. Further studies with multi-parametric imaging using pCASL with dynamic contrast MR imaging [34–35], diffusion kurtosis imaging [36], proton MR spectroscopy [37] and diffusion tensor imaging [38–42] will improve the results. Third, only a single observer measured TBF and ADC of parotid tumors. Further studies with image analysis by multiple observers with the assessment of inter and inter-observer agreement. Forth, the spectrum of the present study cohort is narrow and is composed of PA and WT for benign; and mucoepidermoid, adenoid cystic, and salivary duct carcinomas for malignant tumors. Further multicenter studies upon a large number of patients with different histopathological subtypes will improve the results and can be used in the clinics in the future.

5. Conclusion

We concluded that multi-parametric MR imaging using pCASL and DWI is useful for differentiating benign parotid tumors from parotid malignancy and PA from WT and TBF helps in differentiating WT from malignancy.

References

[1] Abdel Razek AAK, Mukherji SK. Imaging of posttreatment salivary gland tumors. Neuroimaging Clin N Am 2018;28:199–208.
[2] Abdel Razek AAK, Mukherji SK. State-of-the-art imaging of salivary gland tumors. Neuroimaging Clin North Am 2018;28:303–17.
[3] Dai YL, King AD. State of the art MRI in head and neck cancer. Clin Radiol 2018;73:45–59.
[4] Abdel Razek AAK, Mukherji SK. Imaging of minor salivary glands. Neuroimaging Clin North Am 2018;28:295–302.
[5] Bhatia KSS, Dai YL. Routine and advanced ultrasound of major salivary glands. Neuroimaging Clin North Am 2018;28:273–93.
[6] Abdel Razek AA, Ashmalla GA, Gaballa G, et al. Pilot study of ultrasound parotid imaging reporting and data system (PIRADS): inter-observer agreement. Eur J Radiol 2015;85:2533–8.
[7] Miao LY, Xue H, Ge HY, et al. Differentiation of pleomorphic adenoma and Warthin's tumour of the salivary gland: is long-to-short diameter ratio a useful parameter? Clin Radiol 2015;70:1212–9.
[8] Razek AA, Tawfik AM, Elsorogy LG, et al. Perfusion CT of head and neck cancer. Eur J Radiol 2014;38:537–44.
[9] Liang YY, Xu F, Guo Y, et al. Accuracy of magnetic resonance imaging techniques for parotid tumors, a systematic review and meta-analysis. Clin Imaging 2018;52:36–43.
[10] Espinoza S, Felter A, Malinvaud D, et al. Warthin's tumor of parotid gland: surgery or follow-up? Diagnostic value of a decisional algorithm with functional MRI. Diagn Interv Imaging 2016;97:37–43.
[11] Abdel Razek AAK. Routine and advanced diffusion imaging modules of the salivary glands. Neuroimaging Clin North Am 2018;28:245–54.
[12] Attyé A, Troprès I, Rouchy RC, et al. Diffusion MRI: literature review in salivary gland tumors. Oral Dis 2017;23:572–5.
[13] Mikaszewski B, Markiet K, Smugała A, et al. Diffusion-weighted MRI in the differential diagnosis of parotid malignancies and pleomorphic adenomas: can the accuracy of dynamic MRI be enhanced? Oral Surg Oral Med Oral Pathol Oral Radiol 2017;124:95–103.
[14] Razek AAKA. Prediction of malignancy of submandibular gland tumors with apparent diffusion coefficient. Oral Radiol 2019;35:11–5.
[15] Takumi K, Fukukura Y, Hakamada H, et al. Value of diffusion tensor imaging in differentiating malignant from benign parotid gland tumors. Eur J Radiol 2017;95:249–56.
[16] Khalek Abdel Razek AA. Characterization of salivary gland tumours with diffusion tensor imaging. Dentomaxillofac Radiol 2018;47:20170343.
[17] Stefanovic X, Al Tabaa Y, Gascou G, et al. Magnetic resonance imaging of parotid gland tumors: dynamic contrast-enhanced sequence evaluation. J Comput Assist Tomogr 2017;41:541–6.
[18] Abdel Razek AA, Samir S, Ashmalla GA. Characterization of parotid tumors with dynamic susceptibility contrast perfusion-weighted magnetic resonance imaging and diffusion-weighted MR imaging. J Comput Assist Tomogr 2017;41:131–6.
[19] Abdel Razek AAK, Talaat M, El-Serougy L, et al. Clinical applications of arterial spin labeling in brain tumors. J Comput Assist Tomogr 2019;43:525–32.
[20] Abdel Razek AAK, Talaat M, El-Serougy L, et al. Differentiating glioblastomas from solitary brain metastases using arterial spin labeling perfusion- and diffusion tensor imaging-derived metrics. World Neurosurg 2019;127:e593–8.
[21] Razek AAKA, El-Serougy L, Abdelsalam M, et al. Differentiation of residual/recurrent gliomas from postradiation necrosis with arterial spin labeling and diffusion tensor magnetic resonance imaging-derived metrics. Neuroradiology 2018;60:169–77.
[22] Abdel Razek AAK, El-Serougy L, Abdelsalam M, et al. Differentiation of primary central nervous system lymphoma from glioblastoma: quantitative analysis using arterial spin labeling and diffusion tensor imaging. World Neurosurg 2019;123:e303–9.
[23] Fujima N, Kudo K, Tsukahara A, et al. Measurement of tumor blood flow in head and neck squamous cell carcinoma by pseudo-continuous arterial spin labeling: comparison with dynamic contrast-enhanced MRI. J Magn Reson Imaging 2015;41:983–91.
[24] Abdel Razek AAK, Nada N. Arterial spin labeling perfusion-weighted MR imaging: correlation of tumor blood flow with pathological degree of tumor differentiation, clinical stage and nodal metastasis of head and neck squamous cell carcinoma. Eur Arch Otorhinolaryngol 2018;275:1301–7.
[25] Fujima N, Yoshida D, Sakashita T, et al. Usefulness of Pseudocontinuous arterial spin-labeling for the assessment of patients with head and neck squamous cell carcinoma by measuring tumor blood flow in the pretreatment and early treatment period. AJNR Am J Neuroradiol 2016;37:342–8.
[26] Abdel Razek AAK. Arterial spin labelling and diffusion-weighted magnetic resonance imaging in differentiation of recurrent head and neck cancer from post-radiation changes. J Laryngol Otol 2018;132:923–8.
[27] Geerts B, Leclercq D, Tezenas du Montcel S, et al. Characterization of Skull Base lesions using pseudo-continuous arterial spin labeling. Clin Neuroradiol 2019;29:75–86.
[28] Fujima N, Nakamaru Y, Sakashita T, et al. Differentiation of squamous cell carcinoma and inverted papilloma using non-invasive MR perfusion imaging. Dentomaxillofac Radiol 2015;44:20150074.
[29] Yamamoto T, Kimura H, Hayashi K, et al. Pseudo-continuous arterial spin labeling MR images in Warthin tumors and pleomorphic adenomas of the parotid gland: qualitative and quantitative analyses and their correlation with histopathologic and DWI and dynamic contrast enhanced MRI findings. Neuroradiology 2018;60:803–12.
[30] Kato H, Kanematsu M, Watanabe H, et al. Perfusion imaging of parotid gland tumours: usefulness of arterial spin labeling for differentiating Warthin's tumours. Eur Radiol 2015;25:3247–54.
[31] Iida E, Wiggins III RH, Anzai Y. Bilateral parotid oncocytoma with spontaneous intratumoral hemorrhage: a rare hypervascular parotid tumor with ASL perfusion. Clin Imaging 2016;40:357–60.
[32] Abdel Razek A, Elkhamary S, Al-Mesfer S, et al. Correlation of apparent diffusion coefficient at 3 tesla with prognostic parameters of retinoblastoma. Am J Neuroradiol 2012;33:944–8.
[33] Abdel Razek AA, Kamal E. Nasopharyngeal carcinoma: correlation of apparent diffusion coefficient value with prognostic parameters. Radiol Med 2013;118:534–9.
[34] Abdel Razek AA, Gaballa G, Ashamalla G, et al. Dynamic susceptibility contrast perfusion-weighted MR imaging and diffusion-weighted MR imaging in differentiating recurrent head and neck cancer from post-radiation changes. J Comput Assist Tomogr 2015;39:849–54.
[35] Razek AA, Gaballa G, Megahed AS, et al. Time resolved imaging of contrast kinetics (TRICKS) MR angiography of arteriovenous malformations of head and neck. Eur J Radiol 2013;82:1885–91.
[36] Yu J, Zhang Q, Lu Y, et al. Diffusion kurtosis imaging for differentiating parotid tumors. Int J Clin Exp Med 2017;10:8025–30.

[37] Razek AA, Nada N. Correlation of choline/creatine and apparent diffusion coefficient values with the prognostic parameters of head and neck squamous cell carcinoma. NMR Biomed 2016;29:483–9.
[38] Abdel Razek A, Mossad A, Ghonim M. Role of diffusion-weighted MR imaging in assessing malignant versus benign skull-base lesions. Radiol Med 2011;116:125–32.
[39] Abdel Razek AAK, Elkhamary SM, Nada N. Correlation of apparent diffusion coefficient with histopathological parameters of salivary gland cancer. Int J Oral Maxillofac Surg 2019;48:995–1000.
[40] Razek AAA, Ashmalla G. Assessment of paraspinal neurogenic tumors with diffusion-weighted MR imaging. Eur Spine J 2018;27:841–6.
[41] El-Serougy L, Abdel Razek AA, Ezzat A, et al. Assessment of diffusion tensor imaging metrics in differentiating low-grade from high-grade gliomas. Neuroradiol J 2016;29:400–7.
[42] Abdel Razek AA, Soliman N, Elashery R. Apparent diffusion coefficient values of mediastinal masses in children. Eur J Radiol 2012;81:1134–311.